Neutron diffraction, specific heat and magnetic susceptibility of $Ni_3(PO_4)_2$

J. Escobal[a], J.L. Pizarro[b], J.L. Mesa[a],*, J.M. Rojo[a], B. Bazan[b], M.I. Arriortua[b], T. Rojo[a],*

[a]Facultad de Ciencia y Tecnología, Departamento de Química Inorgánica, Universidad del País Vasco, Apdo. 644, E-48080 Bilbao, Spain
[b]Facultad de Ciencia y Tecnología, Departamento de Mineralogía y Petrología, Universidad del País Vasco, Apdo. 644, E-48080 Bilbao, Spain

Abstract

The $Ni_3(PO_4)_2$ phosphate was synthesized by the ceramic method in air atmosphere. The crystal structure consists of a three-dimensional skeleton constructed from Ni_3O_{14} edge-sharing octahedra, which are interconnected by $(PO_4)^{3-}$ oxoanions with tetrahedral geometry. The magnetic behavior was studied on powdered sample by using susceptibility, specific heat and neutron diffraction data. The nickel(II) orthophosphate exhibits a three-dimensional magnetic ordering at approximately 17.1 K. However, its complex crystal structure hampers any parametrization of the J-exchange parameter. The specific heat measurements of $Ni_3(PO_4)_2$ exhibit a three-dimensional magnetic ordering (λ-type) peak at 17.1 K. Measurements above T_N suggest the presence of a small short-range order in this phase. The total magnetic entropy was found to be 28.1 KJ/mol at 50 K. The magnetic structure of the nickel(II) phosphate exhibits ferromagnetic interactions inside the Ni_3O_{14} trimers which are antiferromagnetically coupled between them, giving rise to a purely antiferromagnetic structure.
© 2005 Elsevier Inc. All rights reserved.

Keywords: Nickel(II) phosphate; Susceptibility; Specific heat; Magnetic structure

1. Introduction

The great ability of phosphate frameworks to stabilize different oxidation states is produced for the relatively high charge in $(PO_4)^{3-}$ tetrahedral that favors the formation of anionic frameworks with a high degree of mechanical, chemical, and thermal stability [1,2]. These compounds offer a considerable number of structures which can give rise to original physical properties (magnetic, heterogeneous catalysis, ion exchange, optical, etc.) with potential applications.

A large number of distinct structural types for compounds represented as $M_3P_2O_8$ are known. Amongst these only the sarcopside $Fe_3(PO_4)_2$ structure [3] is based upon a close-packed array of oxygen atoms.

In fact this structure is olivinite-like [4] with vacant cation site ordered and results in a change from an orthorhombic to a monoclinic cell. Joubert et al. [5] have shown that a metastable sarcopside-like structure can be formed by the reaction of olivinite-like $Li_2M_2P_2O_8$ plus MSO_4, with M = Mg or Co at reaction temperatures of 933 and 953 K, respectively.

The crystal structure of the $Ni_3(PO_4)_2$ phase is isotypic with that of sarcopside, which is related to that of olivine with vacant cation sites ordered [6]. This compound crystallizes in the monoclinic $P2_1/c$ space group. The compound exhibits a three-dimensional crystal structure constructed from trimeric $Ni(2)O_6$–$Ni(1)O_6$–$Ni(2)O_6$ edge-sharing octahedra interconnected through the $(PO_4)^{3-}$ oxoanions.

Magnetic measurements of $Ni_3(PO_4)_2$ performed several years ago in the ZFC mode by using a DSM 8 magnetometer/susceptometer were reported [7]. The results indicate the existence of 3D antiferromagnetic

*Corresponding authors. Fax: +34 946013500.
E-mail addresses: qipmeruj@lg.ehu.es (J.L. Mesa),
teo.rojo@ehu.es (T. Rojo).

couplings below, approximately, 18.0 K, but it was not possible to fit the magnetic data to a three-dimensional model. In the related $(Ni_xMg_{3-x})(PO_4)_2$ ($x = 1, 1.5, 2$) series of compounds it was observed that the substitution of Ni^{2+} by the diamagnetic Mg^{2+} ions shifts the susceptibility maximum towards lower temperatures, increasing the paramagnetic domain [7]. However, the substituted phases appear to retain the three-dimensional antiferromagnetic ordering. Three-dimensional antiferromagnetic structure, determined at 2 K by neutron diffraction, with a $T_N = 22.2(5)$ K was also observed in the stoichiometrically $Cu_3(PO_4)_2$ related compound which crystallizes in the triclinic $P-1$ space group [8].

As a part of our research in the field of phosphate and arsenate compounds [9–15] we, here, report on the magnetic, specific heat measurements together with the magnetic structure of the nickel(II) orthophosphate.

2. Experimental

The $Ni_3(PO_4)_2$ phase was synthesized by solid state reaction in air atmosphere starting from $Ni(NO_3)_2 \cdot 6H_2O$ and $(NH_4)(H_2PO_4)$. Stoichiometric quantities of these materials were ground together in an agate mortar. The resulting mixture was heated in an open crucible at 300 °C to decompose all initial reactants. This process was followed by further heating at 800 °C for 20 h with an intermediate regrinding after 10 h. The final product was quenched to room temperature. The obtained compound was cleaned with water and dried over P_2O_5 for 24 h. The contents of Ni and P in the microcrystalline powdered sample was confirmed by inductively coupled plasma atomic emission spectroscopy (ICP-AES).

X-ray powder diffraction patterns were collected on a PHILIPS X'PERT automatic diffractometer operating at 40 kV and 40 mA. $CuK\alpha$ radiation ($\lambda = 1.5418$ Å) was employed with steps of $0.02°$ in 2θ and a fixed time counting of 5 s. The X-ray powder diffraction data were used to evaluate the purity of the product obtained in the synthesis. The data were fitted with the Rietveld method using the FULLPROF program [16,17]. For the $Ni_3(PO_4)_2$ phosphate the monoclinic unit cell, the $P2_1/c$ space group, and the fractional coordinates previously determined from X-ray single crystal data by Calvo et al. [6] were used. The X-ray refined lattice parameters are $a = 5.827(1)$, $b = 4.696(1)$, $c = 10.106(1)$ Å, $\beta = 91.13(1)°$. The reported parameters in Ref. [6] are $a = 5.830(2)$, $b = 4.700(2)$, $c = 10.107(4)$ Å, $\beta = 91.22(2)°$.

Neutron powder diffraction patterns were collected at room temperature on the high resolution D2B powder diffractometer ($\lambda = 1.594$ Å) at the Institut Laue-Langevin in Grenoble. About 5 g of $Ni_3(PO_4)_2$ were

employed in the experiments, placed in a cylindrical vanadium container and held in a liquid helium cryostat. Extensive and accurate diffraction data at room temperature and 1.5 K were recorded over a large angular range $0 \leqslant 2\theta \leqslant 160°$. The data were fitted using the FULLPROF program [17]. Both diffractograms were fitted with a six polynomial background using the pseudo-Voight function to generate the line shape of the diffraction peaks. The 1.5 K pattern was treated refining simultaneously the magnetic and nuclear contributions. The refined lattice parameters were $a = 5.824(1)$, $b = 4.694(1)$, $c = 10.101(1)$ Å, $\beta = 91.13(1)°$ for 300 K and $a = 5.814(1)$, $b = 4.689(1)$, $c = 10.084(1)$ Å, $\beta = 91.16(1)°$ for 1.5 K.

Magnetic susceptibility measurements were performed on polycrystalline sample between 5.0 and 300 K, using a Quantum Design MPSM-7 magnetometer with a magnetic field of 0.1, 0.05 and 0.01 T, at which the magnetization vs. magnetic field is linear even at 5.0 K. Heat capacity measurements were carried out between 1.8 and 100 K by a relaxation method using a PPMS system. The sample was a plate of 0.3 mm thickness and 7 mg weight obtained by compressing the original powder.

3. Results and discussion

3.1. Magnetic behavior

The magnetic measurements of the $Ni_3(PO_4)_2$ compound were recorded in the FC and ZFC modes using a Quantum Design MPSM-7 magnetometer at values of 0.1, 0.05 and 0.01 T (Fig. 1). The results obtained at 0.1 T from room temperature down to 5 K are shown in Fig. 2. A maximum in the molar magnetic susceptibility is observed a 17.1 K indicating the existence of 3D
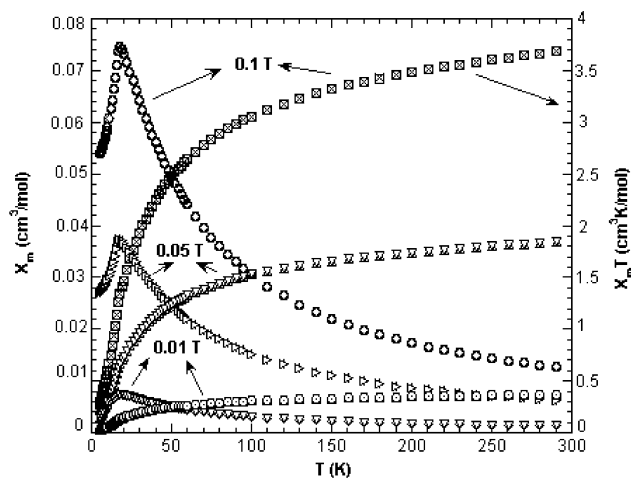

Fig. 1. Thermal evolution of the χ_m and $\chi_m T$ vs. T curves at different magnetic fields in the ZFC and FC modes of $Ni_3(PO_4)_2$.
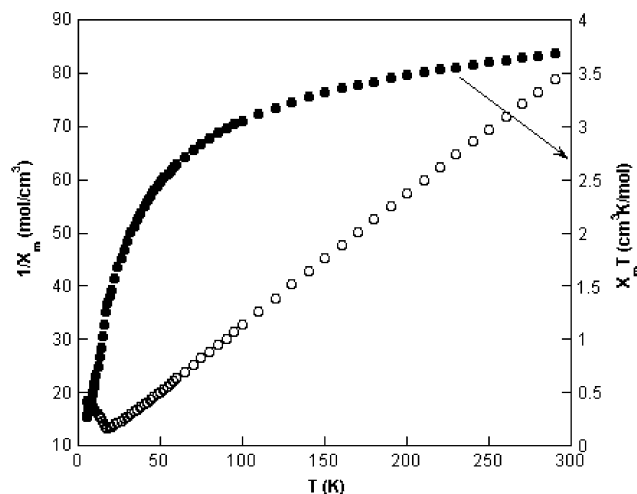
Fig. 2. Thermal evolution of the $1/\chi_m$ and $\chi_m T$ vs. T. curves at 0.1 T of $Ni_3(PO_4)_2$.

antiferromagnetic interactions in good agreement with the structural data. From the magnetic measurements performed at different magnetic fields, it was observed that the thermal evolution of the molar magnetic susceptibility does not show any irreversibility at low temperatures indicating a purely antiferromagnetic behavior of $Ni_3(PO_4)_2$ (see Fig. 1). The values of the Curie and Curie–Weiss constants, $4.08\,cm^3\,K\,mol^{-1}$ and $\theta = -33.3\,K$, respectively, are similar to those previously calculated [7]. The g-value obtained from the Curie constant in the paramagnetic region $[C_m = (Ng^2\mu_B S(S+1))/3K]$ is $g = 2.33$, characteristic of Ni(II) cations in octahedral geometry [18]. The effective magnetic moment calculated from the Curie constant is $3.29\,\mu_B$, in the range habitually found for the Ni(II) (d^8) cations [18]. The $\chi_m T$ vs. T curves decreases from $3.66\,cm^3\,K\,mol^{-1}$ at room temperature to $0.28\,cm^3\,K\,mol^{-1}$ at 5 K, in good agreement with the existence of antiferromagnetic interactions.

Taking into account the three dimensional crystal structure of this phase, attempts to calculate the J-exchange parameter using the Rushbrooke and Wood equation for a 3D antiferromagnetic system [19] were unsuccessful.

3.2. Specific heat measurements

The observed calorimetric results for $Ni_3(PO_4)_2$ carried out in the 1.8–60 K temperature range were evaluated in terms of the molar heat capacity under constant pressure C_p and its temperature variation is shown in Fig. 3. The heat-capacity measurements exhibit three-dimensional magnetic ordering peaks at 17.1 K. The temperature at which this (λ-type) peak appears is similar to that obtained from the magnetic susceptibility measurements. To estimate the magnetic
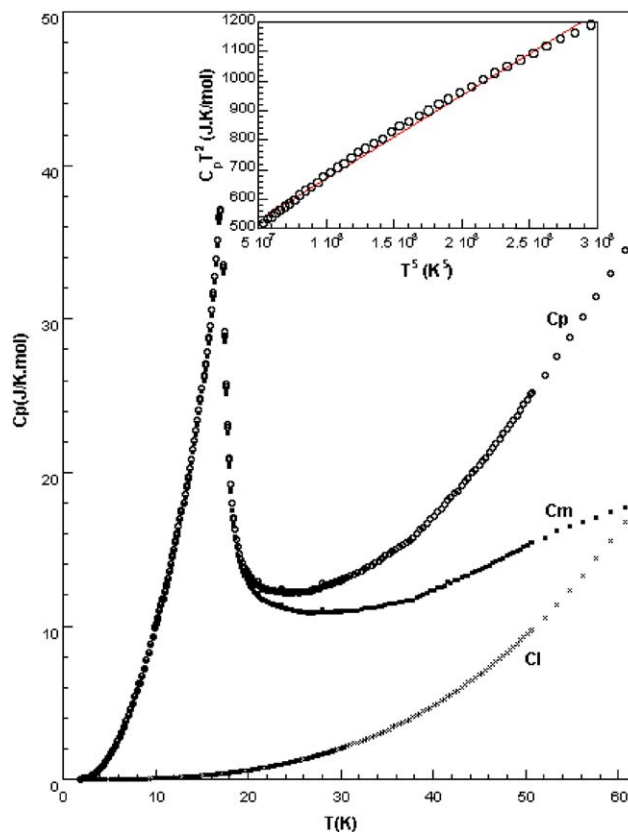

Fig. 3. Specific heat (C_p) of $Ni_3(PO_4)_2$. C_l and C_m are the estimated lattice and magnetic contributions, respectively. The inset shows the $C_p T^2$ vs. T^5 line.

heat capacities C_{mag}, the observed C_p values within the range 35–50 K, above the magnetic phase transition temperature T_N, can be expressed by the sum of the lattice heat capacities, C_p (lattice) and the magnetic heat capacities due to short-range order, C_{mag} (short-range order). Heat capacities of a non-magnetic analogue are often used for determination of lattice heat capacities. Alternatively, these latter are determined mainly either by effective frequency distribution method [20] or by a temperature polynomial [21], in which comparison is made with the observed heat capacity data unaffected by phase transition. From the specific-heat plot, C_p (lattice) can be expressed by a temperature polynomial with cubic and higher order terms, while C_{mag} (short-range order) can be expressed by a term proportional T^{-2} [22]. Thus, the observed heat capacities within 35–50 K range can be described as $C_p = C_p(\text{lattice}) + C_{mag}$ (short-range order) $= \sum_{i=1}^{n} A_i T^i + B T^{-2}$. The observed heat capacity data were well fitted with the first term assuming a Debye model (AT^3) ascribed to the phonons whereas the second one deals with the two-dimensional magnetic correlations (Schottky-type anomaly) [23]. A linear plot of CT^2 vs. T^5 allowed the evaluation of the $A = 7.737 \times 10^{-5}\,JK^{-4}\,mol^{-1}$ and $B = 69233\,JK\,mol^{-1}$
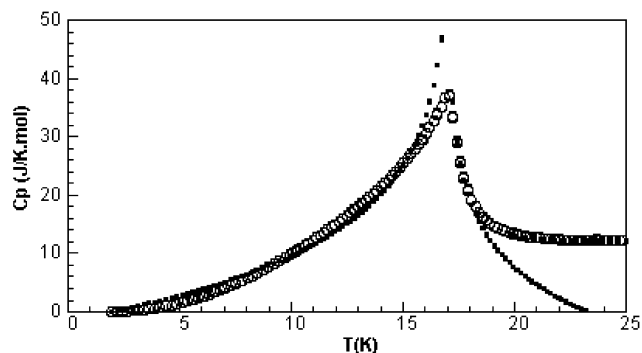
Fig. 4. The heat capacity of $Ni_3(PO_4)_2$ in the neighborhood of the ordering temperatures. The solid circles correspond to the $T < T_N$ and $T > T_N$ equations (see text).

Fig. 5. Magnetic entropy of $Ni_3(PO_4)_2$ as a function of temperature. The horizontal solid line represents the ΔS maximum. The vertical solid line indicates the ordering temperature.

constants (see inset in Fig. 3). The lattice heat capacity curve thus determined for estimating the magnetic heat capacities is shown in Fig. 4. The C_{mag} values were calculated by subtracting the lattice heat capacities from the observed C_p values. An anomaly can now be seen above 40 K as a broad shoulder in the magnetic heat capacity. This fact suggests that a large amount of short-range order between the trimeric NiO_6 octahedra and within planes is present, as might be expected from the structural features. These results are in good agreement with those obtained from susceptibility measurements where a weak decrease in the $\chi_m T$ vs. T curve is observed.

Considering the λ-type maximum observed in the heat capacity measurements, a fit near the ordering temperatures following the equation $C_m = \alpha - \beta T \operatorname{Ln}|T - T_N|$ given by Kopinga et al. [24] was carried out. The magnetic specific-heat data plotted versus $\operatorname{Ln}|T - T_N|$ for $T_N = 17.1$ K show linear behavior below and above the ordering temperature. The values near the transition point, T_N, satisfy the equation $C_m = 34.5 - 12.7 \operatorname{Ln}|17.1 - T|$ and $C_m = 18.5 - 10.1 \operatorname{Ln}|T - 17.1|$ for $T < T_N$ and $T > T_N$, respectively. These equations are described by the solid circles given in Fig. 4 and show the presence of short-range interactions above the ordering temperature.

The magnetic entropy at 50 K, $S_m = \int (C_m/T) dT$, is $3.41R$ (Fig. 5). The small differences of the experimental entropy with respect to the theoretical value of $3.29R$ for an $S = 1$ system could be originated by the procedure to calculate the lattice contribution, which is approximated. An amount of $1.7R$ (52%) of the experimental entropy was gained below the ordering temperature, $T_N = 17.1$ K. The rest of entropy could be attributed to the short-range interactions associated to the magnetic exchange interactions inside the Ni(II) trimers. The obtained value is similar to those observed in other three-dimensional phosphate systems [24].

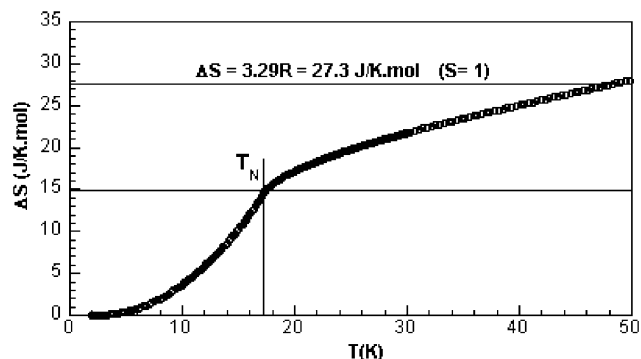### 3.3. Nuclear structure

The room temperature D2B powder diffraction pattern ($\lambda = 1.594 \, \text{Å}$) was refined using the Rietveld method taking as starting model the crystal structure of $Ni_3(PO_4)_2$ [6]. The diffractograms at 300 and 1.5 K are shown in Fig. 6. The room temperature structural parameters and reliability factors from D2B data refinement are summarized in Table 1. The final refined positional and thermal parameters are given in Table 2. The interatomic bond distances and angles are included as supplementary material.

The crystal structure of $Ni_3(PO_4)_2$ is shown in Fig. 7. In this compound the two NiO_6 octahedra show Ni–O distances ranging from 2.092(2) to 2.070(2) Å and from 2.037(2) to 2.185(2) Å for $Ni(1)O_6$ and $Ni(2)O_6$ octahedra, respectively. In the $Ni(1)O_6$ octahedron the *trans*-O–Ni–O angles are of 180°, due to the special position of the Ni(II) cations on an inversion center. The *cis*-O–Ni–O angles range from 72.0(1)° to 108.0(1)°. The $Ni(2)O_6$ octahedron is more irregular and the *trans*- and *cis*-O–Ni–O angles range from 156.8(1)° to 172.3(1)° and from 68.9(1)° to 113.6(1)°, respectively. In the crystal structure only one crystallographically independent $(PO_4)^{3-}$ oxoanion exists. The mean P–O bond distance is 1.55(3) Å. These results are in good agreement with those obtained by Calvo et al. from X-ray single crystal diffraction data [6].

3.4. Low-temperature neutron diffraction

The low temperature pattern at 1.5 K exhibits extra magnetic peaks, indicating that the compound is magnetically ordered (see Fig. 6).

The magnetic peaks can only be indexed considering a magnetic lattice in which the unit-cell parameters are duplicated with respect to those of the nuclear one, with a propagation vector of [1/2,1/2,1/2]. Consequently, the volume of the magnetic cell is eight times larger than
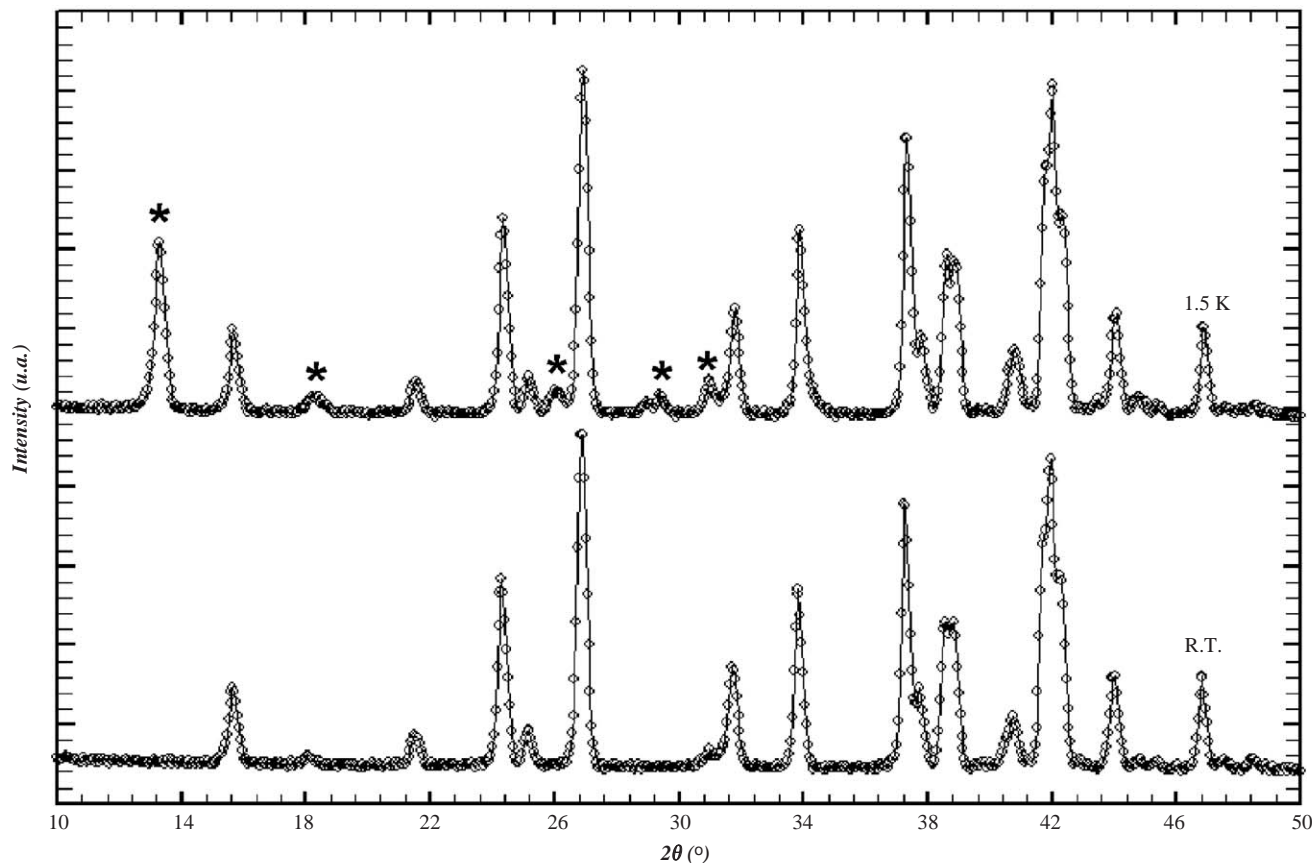
Fig. 6. D2B neutron diffraction diagrams of $Ni_3(PO_4)_2$ at room temperature and 1.5 K. Magnetic contributions are marked (*).

Table 1
Details of Rietveld refinement from D2B neutron diffraction pattern at 300 and 1.5 K for $Ni_3(PO_4)_2$

Temperature (K)	300	1.5
Molecular weight ($g\,mol^{-1}$)	366.1	
Crystal system	Monoclinic	
Space group	$P2_1/c$ (No. 14)	
Angular range (deg.)	11.0–150.0	14.0–148.0
a/Å	5.824(1)	5.814(1)
b/Å	4.694(1)	4.689(1)
c/Å	10.101(1)	10.084(1)
β/°	91.134(1)	91.160(1)
V/Å^3	276.06(1)	274.86(1)
Reliability factors (%)		
$R_p = \Sigma|yi_{obs}—(1/c)yi_{calc}|/\Sigma yi_{obs}$	3.56	4.28
$R_{wp} = [\Sigma wi|yi_{obs}—(1/c)yi_{calc}|^2/\Sigma wi[yi_{obs}]^2]^{1/2}$	4.42	5.53
$R_B = \Sigma|I_{obs}—I_{calc}|/\Sigma I_{obs}$	2.93	2.75
GOF	2.89	3.82

Table 2
Atomic coordinates and thermal parameters for $Ni_3(PO_4)_2$ from D2B neutron diffraction data at 300 and 1.5 K (*Italics*)

Atom	Wyckoff position	x	y	z	B
Ni(1)	2b	0.5	0.0	0.0	0.80(1)
		0.5	*0.0*	*0.0*	*0.52(1)*
Ni(2)	4e	0.2416(2)	−0.0145(2)	0.2746(1)	0.80(1)
		0.2420(2)	*−0.0144(2)*	*0.2742(1)*	*0.52(1)*
P	4e	0.2500(3)	0.4222(4)	0.0945(2)	0.59(3)
		0.2503(4)	*0.4222(4)*	*0.0945(2)*	*0.49(1)*
O(1)	4e	0.2667(3)	0.7466(3)	0.1019(2)	0.80(1)
		0.2669(3)	*0.7470(4)*	*0.1014(2)*	*0.49(1)*
O(2)	4e	0.2566(3)	0.1928(3)	0.4517(2)	0.80(1)
		0.2563(3)	*0.1929(4)*	*0.4512(2)*	*0.49(1)*
O(3)	4e	0.0507(3)	0.3003(3)	0.1729(2)	0.80(1)
		0.0498(3)	*0.2999(4)*	*0.1728(2)*	*0.49(1)*
O(4)	4e	0.4655(3)	0.2651(4)	0.1621(2)	0.80(1)
		0.4659(3)	*0.2656(4)*	*0.1621(2)*	*0.49(1)*

that of the nuclear unit-cell. The six Ni(II) magnetic atoms belonging to the nuclear unit-cell occupy two independent crystallographic positions in the $P2_1/c$ space group. The Ni(1) ions (named S) are in a 2b special position (inversion center) and are numbered (1) $\frac{1}{2}$, 0, 0 and (2) $\frac{1}{2}$, $\frac{1}{2}$, $\frac{1}{2}$. The Ni(2) ions (named R) are located in a 4e general position and are numbered (1) x, y, z; (2) $-x, \frac{1}{2}+y, \frac{1}{2}-z$; (3) $-x, -y, -z$; (4) $x, \frac{1}{2}-y, \frac{1}{2}+z$. So,
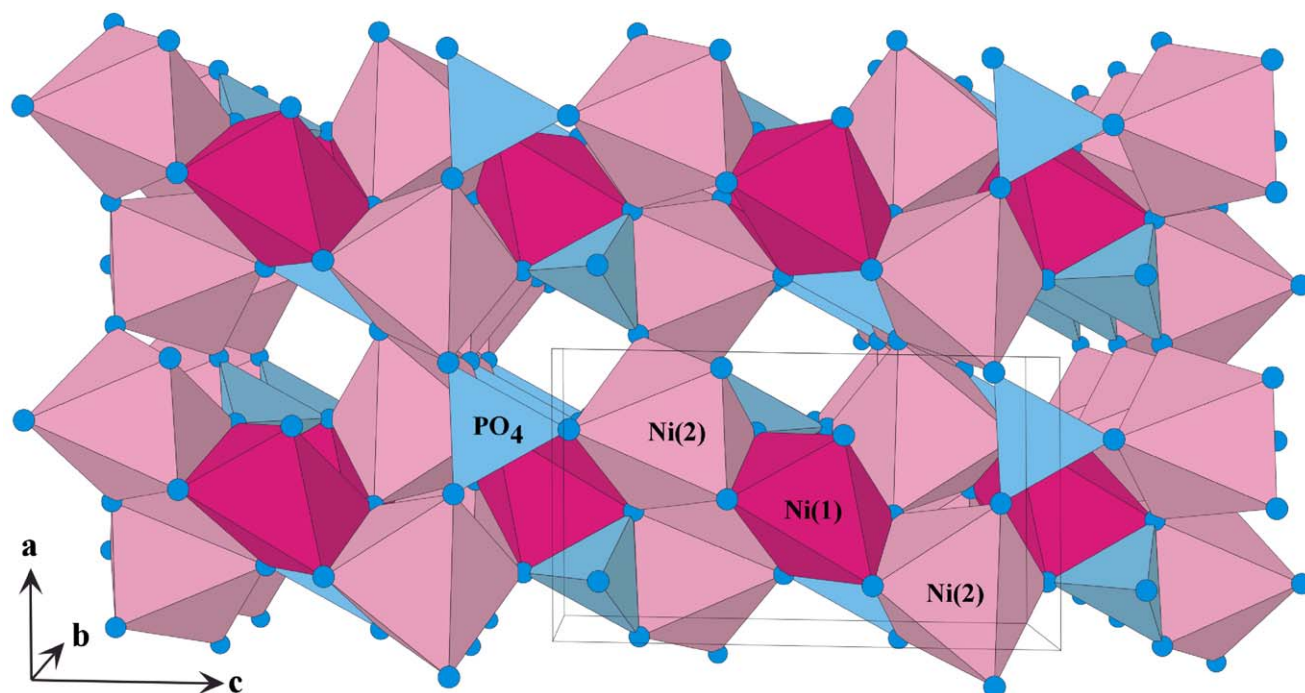
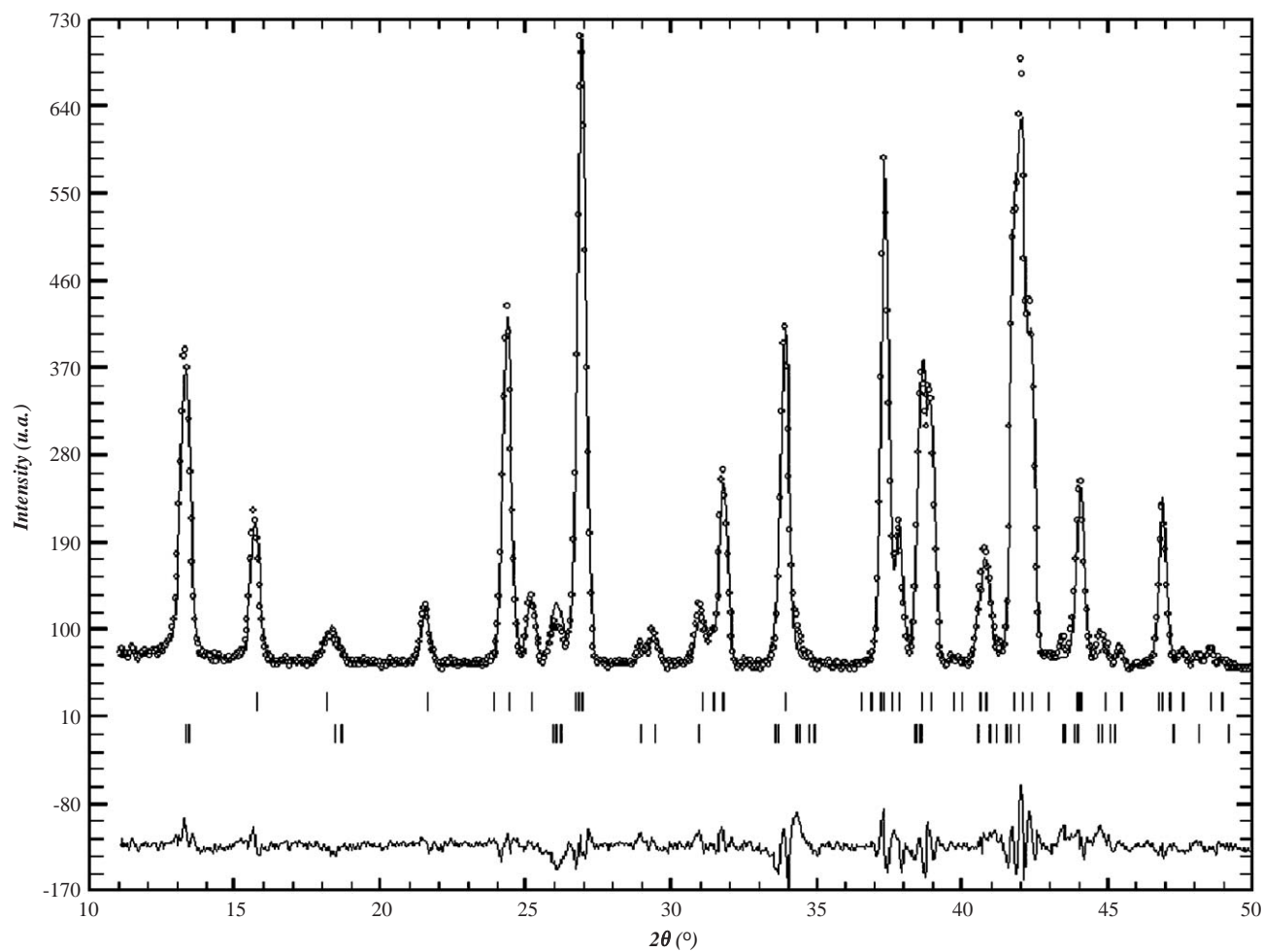Fig. 7. Polyhedral view of the crystal structure of $Ni_3(PO_4)_2$ along the [010] direction.

Fig. 8. Refinement of D2B neutron diffraction profil at 1.5 K ($\lambda = 1.594$ Å). The positions of the Bragg reflections for the nuclear (top) and magnetic (bottom) structures are presented. The difference curves are plotted at the bottom of the figure with the same scale.

48 Ni(II) cations in the magnetic unit-cell appear. This large number of magnetic ions hampers the use of the Bertaut macroscopic theory [25] to deduce the magnetic structure of $Ni_3(PO_4)_2$.

The six Si and Ri magnetic atoms in the nuclear unit cell form two equivalent face-sharing octahedral trimers (R1:S1:R3 and R2:S2:R4) with a common

vertex. The possible magnetic models were analyzed performing a profile analysis of the pattern recordered at 1.5 K by using the Rietveld method (FULLPROF program), between $11.0°$ and $50°$ in 2θ (Fig. 8), and including two phases: the nuclear contribution and a magnetic one. This analysis was carried out taking into account the different possible
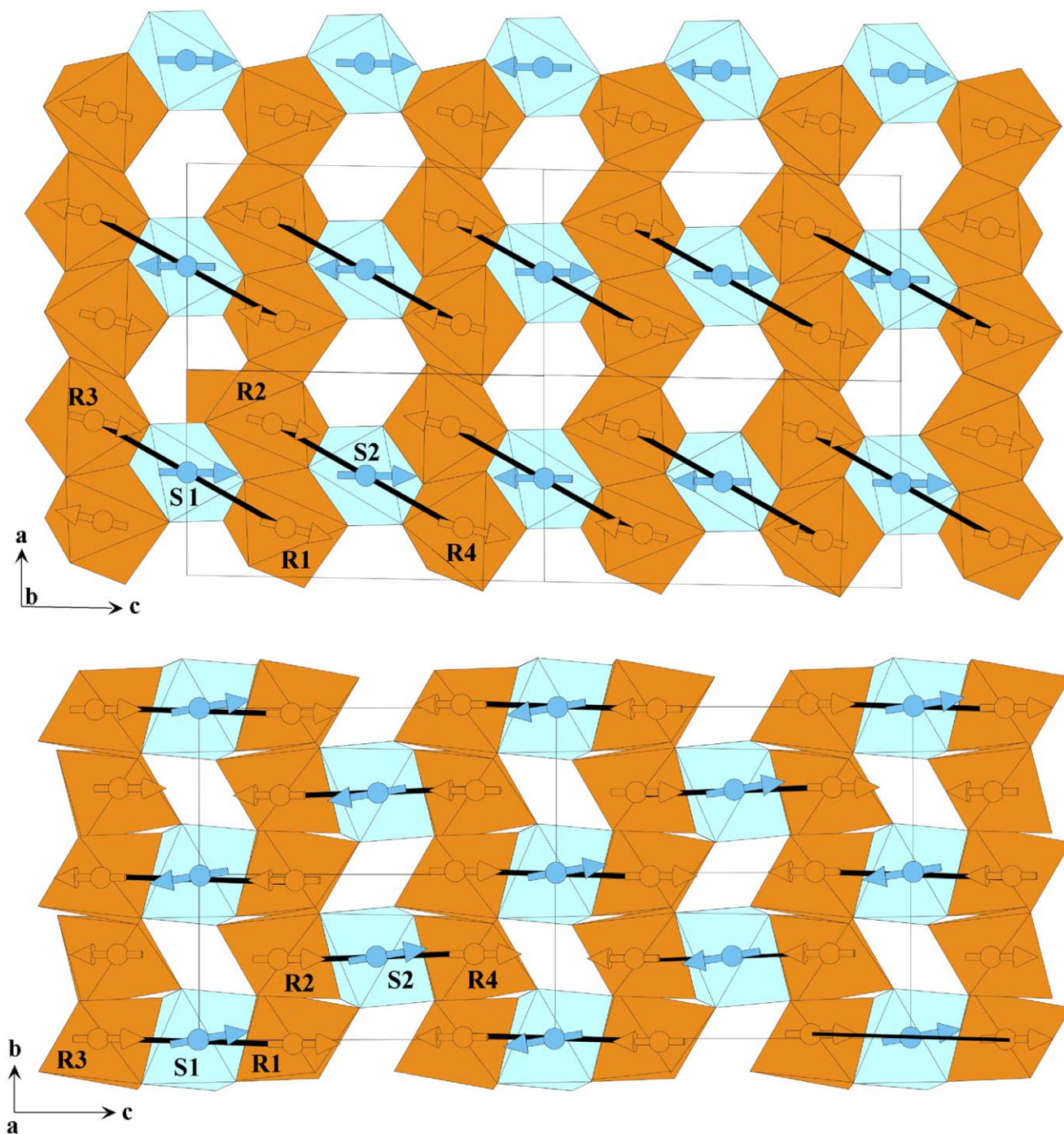

Fig. 9. Orientation of the the Ni(1) [S] and Ni(2) [R] moments in the magnetic structure of $Ni_3(PO_4)_2$ along the [010] (up) and [100] (down) directions. The nuclear unit cell has been repeated along the a-, b- and c-axis in order to show the duplication of the magnetic unit cell in the three spatial directions. The Ni_3O_{14} ferromagnetic trimers are marked with a solid line.

spin arrangements for the second magnetic phase that permit to obtain a purely antiferromagnetic structure, as was observed from the magnetic measurements.

The best fit ($R_{mag} = 13.70\%$) was obtained with a magnetic model in which the main Ni(II) moments are ferromagnetically coupled and located in the z-axis, $MS_z = 2.5(2)$ and $MR_z = 2.2(1)\,\mu_B$ (see Fig. 9). In addition, they are small components for both ions, along the y-axis for S ions [$MS_x = 0.0$, $MS_y = 0.8(2)\,\mu_B$] and along the x-axis for R [$MR_x = -1.0(3)$, $M_{Ry} = 0.0\,\mu_B$]. The total magnetic moments obtained for both cations belonging to the crystal structure of this compound are $MS = 2.6(2)$ and $MR = 2.2(1)\,\mu_B$ for the Ni(1) and Ni(2) cations, respectively.

The coupling between the magnetic components inside the trimer are: $-R1x$:(S1x):$-R3x$ and $-R2x$:(S2x):$-R4x$ along the x-axis; (R1y):$+$S1y:(R3y) and (R2y):$+$S2y:(R4y) along the y direction, and $+R1z$:$+$S1z:$+$R3z and $+R2z$:$+$S2z:$+$R4z along the z-axis (the symbols between brackets denote null components). This magnetic model supposes the existence of a ferromagnetic coupling between the Ni(II) cations inside the edge-sharing trimeric octahedra with their moments slightly unaligned. In the nuclear unit-cell there are two ferromagnetic trimers with the spins near to a parallel disposition, generating a net magnetic component of approximately six Ni(II) arranged for the most part along the z direction ($M_x = 4MR_x = -3.2$; $M_y = 2MS_y = 1.6$; $M_z = 2MS_z + 4MR_z = 12.8\,\mu_B$). However, as the propagation vector is $[\frac{1}{2}, \frac{1}{2}, \frac{1}{2}]$ the unit-cell parameters are duplicated in the three axis. Consequently, a change in the sign of the orientations of the magnetic moments in the three spatial directions takes place and all the components of the moments are cancelled establishing a magnetic structure purely antiferromagnetic (see Fig. 9). These results are in good agreement with those obtained from the magnetic measurements.

3.5. Magnetostructural correlations

Considering the structural features of the $Ni_3(PO_4)_2$ orthophosphate (see Fig. 7) three magnetic exchange pathways can take place: (i) superexchange intratrimeric interactions via oxygen involving the d_{x2-y2} metal orbital from edge-sharing trimeric octahedra, (ii) superexchange intertrimer interactions via common oxygen vertex and (iii) superexchange interactions through the $(PO_4)^{3-}$ oxoanions which are linked to the Ni_3O_{14} polyhedra in three dimensions. The shorter nickel–nickel bond distance through the space is 3.183(1) Å, and consequently direct magnetic interactions can be negligible (see Table 3). The magnetic interactions propagated via $(PO_4)^{3-}$ tetrahedra (Ni–O–P–O–Ni) are always antiferromagnetic and are characterized by both the O–P–O, P–O–Ni angles and the Ni–O bond length [26]. The magnetic exchanges are more effective for the shortest Ni–O distances and for angles values near 109° (tetrahedral angle) [27]. In $Ni_3(PO_4)_2$, the mean nickel–oxygen distance is 2.08(1) Å for both the $Ni(1)O_6$ and $Ni(2)O_6$ octahedra, respectively. The P–O–Ni and O–P–O angles range from 91.6(1)° to 125.7(1)° and from 101.8(2)° to 113.3(2)°, respectively (see Table 3). Inside the Ni_3O_{14} trimeric units the Ni–O–Ni bond angles range from 96.781(7)° to 129.20(1)° giving rise to both ferro- or antiferromagnetic interactions (see Table 3). The values of the angles near to 90° could explain [28] the existence of the ferromagnetic ordering observed in the trimeric units, as proposed from the magnetic structure. Finally, the connection between the Ni_3O_{14} units via |PO4| groups, with Ni–O–P–O–Ni bond angles departure from the orthogonal values of 90°, gives rise to the whole antiferromagnetic behavior observed from both the magnetic susceptibility data and the magnetic structure.

4. Concluding remarks

$Ni_3(PO_4)_2$ exhibits three-dimensional antiferromagnetic couplings with a Neel temperature of 17.1 K. The

---

Table 3
Selected bond distances (Å) and angles (°) related to the possible magnetic exchange pathways for $Ni_3(PO_4)_2$ at 1.5 K

Exchange pathways	Ni–Ni distance (Å)	Length of the exchange pathways (Å)	Angles (°)			
Ni(1)–O–P–O–Ni(1)	3.183(1)	6.69(1)	Ni(1)–O(1)–P	125.7(1)	O(1)–P–O(2)	113.1(2)
Ni(2)–O–P–O–Ni(2)	3.183(1)	6.69(1)	Ni(1)–O(2)–P	93.0(1)	O(1)–P–O(3)	113.3(2)
			Ni(2)–O(3)–P	96.7(1)	O(2)–P–O(3)	112.7(2)
			Ni(2)–O(4)–P	91.6(1)	O(3)–P–O(4)	101.8(2)

Bond angles (°) in the Ni_3O_{14} trimeric units
Ni(1)–O(1)–Ni(2)	99.385(8) **(F)**
Ni(1)–O(2)–Ni(2)	123.780(8) **(AF)**
Ni(2)–O(3)–Ni(2)	128.46(1) **(AF)**
Ni(1)–O(4)–Ni(2)	96.781(7) **(F)**
Ni(1)–O(4)–Ni(2)	116.711(8) **(AF)**
Ni(2)–O(4)–Ni(2)	129.20(1) **(AF)**

specific heat data show a 3D magnetic ordering peak (λ-type) at 17.1 K. Approximately a 52% of entropy estimated at 50 K is gained below the ordering temperature, being the rest attributed to the short-range magnetic interactions inside the nickel(II) trimers. The neutron diffraction pattern at 1.5 K exhibits extra magnetic peaks indicating that the compound is magnetically ordered at low temperatures. The magnetic structure is consistent with an antiferromagnetic phase with the presence of ferromagnetic couplings in the trimer units.

Acknowledgments

Appendix A. Supplementary materials

The online version of this article contains additional supplementary data. Please visit doi:10.1016/j.jssc.2005.06.022

References

[1] R.C. Haushalter, L.A. Mundi, Chem. Mater. 4 (1992) 31.
[2] A. Clearfield, Chem. Rev. 88 (1988) 125.
[3] P.B. Moore, Am. Miner. 57 (1972) 24.
[4] L.W. Fingers, Am. Crystallogr. Assoc. Summer Meeting, Carleton University, Ottawa, Canada, 1970, p. 66.
[5] J.C. Joubert, G. Berthet, E.F. Bertaut, Z. Kristallogr. 136 (1972) 98.
[6] C. Calvo, R. Faggiani, Can. J. Chem. 53 (1975) 1516.
[7] T. Rojo, L. Lezama, J.M. Rojo, M. Insausti, M.I. Arriortua, G. Villeneuve, Eur. J. Solid State Inorg. Chem. 29 (1992) 217.
[8] J.B. Forsayth, C. Wilkinson, S. Paster, H. Effenberger, J. Phys: Condens. Matter 2 (6) (1990) 1609.
[9] J.M. Rojo, J.L. Mesa, L. Lezama, T. Rojo, J. Mat. Chem. 7 (11) (1997) 2243.
[10] J.M. Rojo, J.L. Mesa, R. Calvo, L. Lezama, R. Olazcuaga, T. Rojo, J. Mat. Chem. 8 (6) (1998) 1423.
[11] J.L. Mesa, J.L. Pizarro, L. Lezama, J. Escobal, M.I. Arriortua, T. Rojo, J. Solid State Chem. 141 (1998) 508.
[12] J.M. Rojo, J.L. Mesa, L. Lezama, T. Rojo, J. Solid State Chem. 145 (1999) 629.
[13] J.L. Mesa, A. Goñi, L. Lezama, J.L. Pizarro, R. Olazcuaga, T. Rojo, Ann. Chim. Sci. Mat. (1999) S21.
[14] A. Goñi, L. Lezama, J.L. Pizarro, J. Escobal, M.I. Arriortua, T. Tojo, Chem. Mater. 11 (1999) 1752.
[15] J.L. Mesa, A. Goñi, A.L. Brandl, O. Moreno, G.E. Barberis, T. Rojo, J. Mat. Chem. 10 (2000) 2779.
[16] H.M. Rietveld, J. Appl. Crystallogr. 2 (1969) 65.
[17] J. Rodriguez-Carvajal, Physica B 192 (1993) 55.
[18] R.L. Carlin, Magnetochemistry, Springer, Berlin, 1986.
[19] G.S. Rushbrooke, P.J. Wood, Mol. Phys. 6 (1932) 409.
[20] M. Sorai, S. Seki, J. Phys. Soc. Japan 32 (1972) 382.
[21] T. Matsumoto, Y. Miyazaki, A.S. Albrecht, C.P. Landee, M.M. Turnbull, M. Sorai, J. Phys. Chem. B 79 (1975) 427.
[22] H.M.J. Blöte, Physica B 79 (1975) 427.
[23] P. Rabu, S. Angelov, P. Legoll, M. Belaiche, M. Drillon, Inorg. Chem. 32 (1993) 2463.
[24] K. Kopinga, P.W.M. Borm, W.J.M. De Jonge, Phys. Rev. B 10 (11) (1974) 4690.
[25] E.F. Bertaut, Acta Crystallogr. A 24 (1968) 217.
[26] J.M. Mays, Phys. Rev. 131 (1963) 38.
[27] P.W. Anderson, Magnetism, Academic Press, San Diego, 1963.
[28] J.B. Goodenough, Magnetism and the Chemical Bond, Interscience, New York, 1963.